

## WELL TRAP STRUCTURES AND BULK-NANO ENVIRONMENT LUMINESCENCE CENTERS IN $\text{CaZnGe}_2\text{O}_6:\text{Tb}^{3+}$ LONG AFTERGLOW PHOSPHOR

Boon Kuan Woo<sup>1</sup>, Yang Li<sup>2</sup>, Surinder P. Singh<sup>2</sup>

<sup>1</sup>Department of Physics, University of Texas at Arlington, Arlington, TX 76019-0059, Faculty of Engineering, Multimedia University, Cyberjaya campus, Selangor, Malaysia

<sup>2</sup> Department of Engineering Science and Materials, University of Puerto Rico, Mayaguez, PR 00680, USA

**ABSTRACT** A long afterglow phosphor  $\text{CaZnGe}_2\text{O}_6:\text{Tb}^{3+}$  has been prepared by using organic coated luminescence ZnO nanopowder through a high temperature solid-state reaction route. This new  $\text{CaZnGe}_2\text{O}_6:\text{Tb}^{3+}$  long afterglow phosphor sample emits the  $\text{Tb}^{3+}$  green fluorescence 543 nm emission corresponding to  $^5\text{D}_4 \rightarrow ^7\text{F}_5$  transition under UVA 350 nm illumination. The organic coated luminescence ZnO nanopowder serves to construct shallow well trap for the  $\text{Tb}^{3+}$  dopant and to minimize electron leakage of well traps. By adjusting the mass ratio of both the bulk ZnO powder (<1000 nm size) and the organic coated luminescence ZnO nanopowder (5-10 nm size), depth of well traps that dictate luminescence and afterglow properties could be controlled. The optimized long afterglow phosphor sample was found to be made of 70% gm-weight of bulk ZnO powder and 50% gm-weight of organic coated luminescence ZnO nanopowder or  $\text{CaZn}_{0.83}\text{Ge}_2\text{O}_6:\text{Tb}^{3+}$  phase compound that exhibit afterglow longevity of longer than 3 hours. Therefore, phosphorescence effect is best explained based upon well trap structures model and structure lattice defects play an important role in influencing persistent luminescence phenomena.

**(Keywords:** Afterglow phosphor, phosphorescence, well trap structure .)

---

### INTRODUCTION

In the past decade, research on afterglow phosphor materials that has long decay lifetime has attracted the attention of many researchers. Afterglow phosphor materials have their potential applications in display technology as well as in detection of high energy radiation beams such as X-ray, cathode-ray, UV ray and beta ray [1-5]. Among the many afterglow phosphor materials, so far the rare-earth ions doped alkali earth aluminates and oxysulfide based phosphors have been aggressively explored and utilized broadly. Theoretically, long lasting afterglow phosphor is believed due to thermally stimulated recombination of electrons and holes stored in the traps at room temperature and the afterglow properties depend on the trap density, trap depth and host lattice [6, 7]. However, the exact nature of the trap and the mechanism of capturing and releasing the light energy remain largely unknown, therefore it is in our interest that by making use of our organic coated luminescence ZnO nanopowder [8] in phosphor preparations, we hope to gain a deep

and clear understandings behind the afterglow mechanisms, even though our original goal was

to utilize them for biomedical applications. We devoted our attention to alkali earth germinates based phosphors with  $\text{Tb}^{3+}$  doping as the main activator.

In this paper, we report the observations and the investigations of a new afterglow phosphor that differs from the former contributors [9]. A new approach to prepare afterglow samples was reported by Pan group [10], in which TEOS (tetraethylorthosilicate) and inorganic powders were used as reactants in synthesizing long afterglow phosphor material. However in this paper, we prepared our afterglow phosphor samples by using both the bulk ZnO powder and organic coated luminescence ZnO nanopowder as precursor through high temperature solid-state reaction. The structural and morphological properties of the optimized afterglow phosphor were characterized by using transmission electron microscope (TEM) and scanning electron microscopy (SEM). These new

phosphor materials were thoroughly investigated for their optical and structural properties.

## EXPERIMENTS

### Sample Preparation

The afterglow phosphor powder samples were prepared according to stoichiometric proportions with the following amounts of Germanium (IV) oxide [0.878 gm, 8.4 mmole, 99.998%], Calcium (II) oxide [0.235 gm, 4.2 mmole, 99.9%], Bulk Zinc oxide powder and/or organic coated luminescence ZnO nanopowder [Total mass of 0.342 gm, 4.2 mmole or 100% gm-weight, 99.9% for bulk] and Terbium (III, IV) oxide [0.03 gm, 0.04 mmole, 99.999%, 3.8 mol% Tb<sup>3+</sup>]. All chemicals were obtained and purchased from Sigma-Aldrich with the exception of the organic coated luminescence ZnO nanopowder. All powders were thoroughly mixed together, placed in a covered alumina crucible, pre-heated at 200°C for 1 hour and finally annealed at 1100°C for 1 hour under normal atmospheric condition. Approximately 1.3 gm of hardened white sample in shallow bowl chunk shape was obtained and then crushed into powder form using the mortar and pestle. These afterglow phosphor powder samples were then subjected for further characterizations.

### Characterization

The SEM images were obtained from Hitachi S-3000N Scanning Electron Microscope. The crystalline phase analysis of the afterglow phosphor compounds were carried out on a Bruker X-ray diffractometer with Cu K $\alpha$  ( $\lambda = 1.5406 \text{ \AA}$ ) radiation and high resolution transmission electron microscope (JEOL 2010 TEM) at a working voltage of 200 kV. The TEM specimen was prepared by depositing powders in ethanol solution onto carbon film coated Cu grids, and observed in a JEOL 2010 TEM at a working voltage of 200 kV. The EDS measurements were performed using an Oxford Instruments EDS detector with an INCA energy. The emission and excitation spectra were measured using a Shimadzu RF-5301PC fluorometer. The afterglow decay curve was measured using the same Shimadzu RF-5301PC fluorometer. X-ray luminescence was measured in a light-proof X-ray cabinet equipped with optic fiber connection to an outside detector. X-ray irradiation was performed using a Faxitron RX-650 cabinet (Faxitron X-Ray Corp, IL, USA)

using 60 kV, 12' source-object distance and 5 mm distance optic-fiber to object, at 135°. The luminescence spectra were recorded using a QE65000 spectrometer (Ocean Optics Inc, Dunedin, FL), connected to the X-ray chamber using a 600  $\mu\text{m}$  core diameter, P600-2-UV-Vis fiber optic (Ocean Optics Inc, Dunedin, FL).

## RESULTS AND DISCUSSION

**Figure 1(a)** shows a TEM image of a grain particle of the afterglow sample made from 100% gm-weight organic coated luminescence ZnO nanopowder. From the magnified high-resolution TEM (HRTEM) images in (b-d), it is estimated that the near squared lattice spacing in the particle to be 1 nm which corresponds to (100) and (010) planes, respectively, along the [001] zone axis. **Figure 1(e)** is the electron diffraction pattern of the [001] zone axis, where the reflection conditions are:  $h = 2n$  for  $h00$ , and  $k = 2n$  for  $0k0$ , where  $n$  is an integer. Some visible reflections at the forbidden sites are formed by double reflections. The reflection conditions are consistent to its space group  $C2/c$ . The EDS data in **Figure 1(f)** clearly indicates that terbium atoms have been successfully doped into CaZnGe<sub>2</sub>O<sub>6</sub> host lattice and with no traces of carbon impurities.

The best possible mechanism to explain long lasting afterglow is based upon the nature of well traps [11-18]. Samples with shallow well traps tend to give short burst of afterglow while samples with very deep well traps may not give phosphorescence at all at room temperature. The best approach is to fabricate samples with middle-size depth well traps by combining both the shallow well traps and deep well traps. However, this is only possible if we could identify the key elements that could construct physical well trap structure within the host lattice material. In our study of CaZnGe<sub>2</sub>O<sub>6</sub>:Tb<sup>3+</sup> phosphorescence material, we found that the crucial well-building material is zinc oxide. First, 3 samples were made with 100% gm-weight from bulk ZnO powder, commercially available ZnO nanopowder and organic coated luminescence ZnO nanopowder. Their physical and optical properties were observed and compared. We observe that samples made from bulk ZnO powder and ZnO nanopowder exhibited same physical appearances and optical properties while the sample made from organic coated luminescence ZnO nanopowder gives us

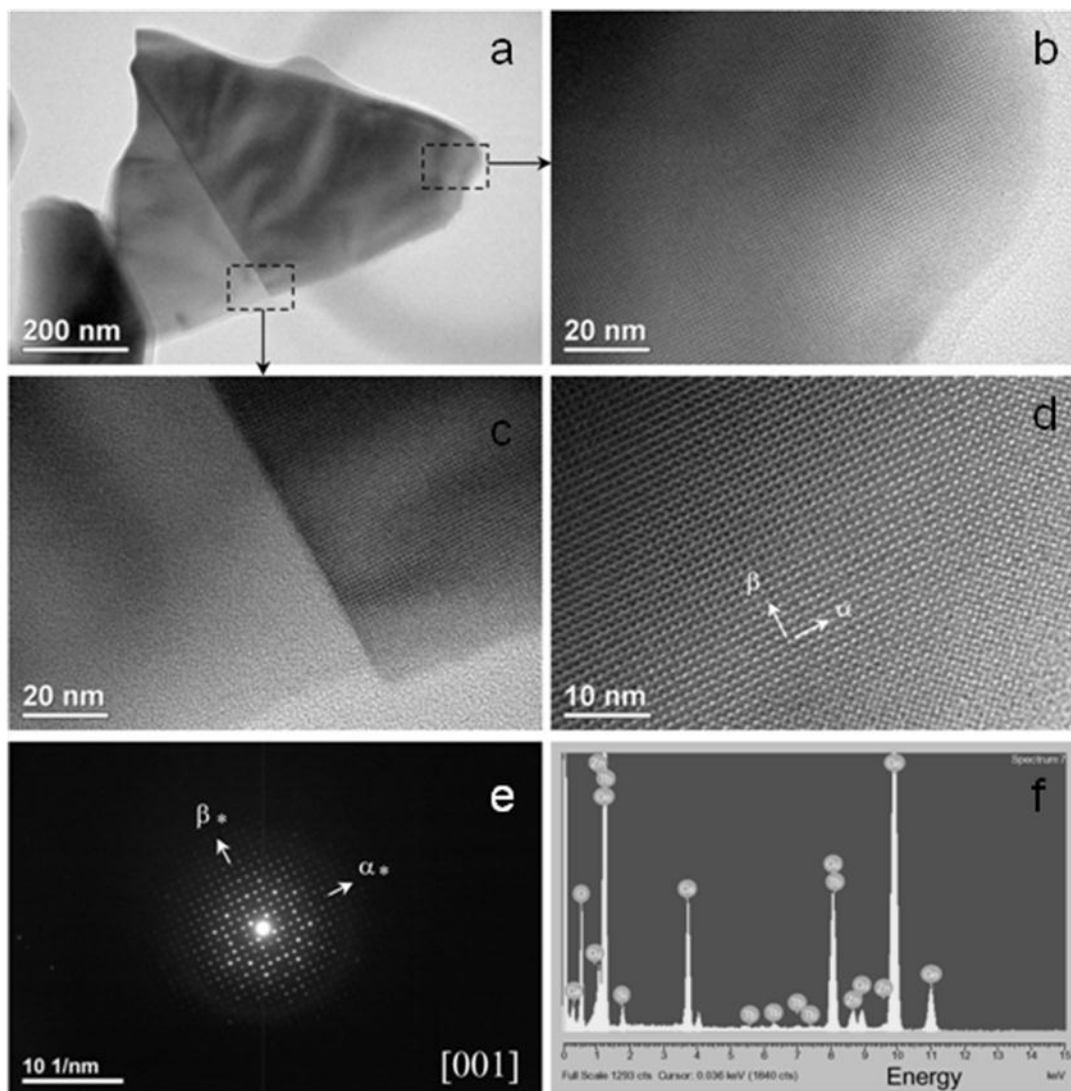


Figure 1. TEM/EDS data on  $\text{CaZnGe}_2\text{O}_6:\text{Tb}^{3+}$  afterglow phosphor made of 100% gm-weight organic coated luminescence ZnO nanopowder.

different optical properties, not yet reported before. **Figure 2** shows us the optical properties of  $\text{CaZnGe}_2\text{O}_6:\text{Tb}^{3+}$  made of 100% gm-weight organic coated luminescence ZnO nanopowder as compared to sample made of 100% gm-weight bulk ZnO. This new emerging seven excitation peaks (303 nm, 317 nm, 339 nm, 353 nm, 369 nm, 379 nm and 486 nm corresponding to  ${}^7\text{F}_6-{}^3\text{H}_6$ ,  ${}^7\text{F}_6-{}^5\text{D}_0$ ,  ${}^7\text{F}_6-{}^5\text{L}_7$ ,  ${}^7\text{F}_6-{}^5\text{L}_9$ ,  ${}^7\text{F}_6-{}^5\text{G}_5$ ,  ${}^7\text{F}_6-{}^5\text{G}_6$  and  ${}^7\text{F}_6-{}^5\text{D}_4$  transitions of  $\text{Tb}^{3+}$ , respectively) has us convinced that the organic coated luminescence ZnO nanoparticles are responsible for constructing the shallow well traps in this afterglow phosphor material. Beside, revealing the 4f to 5d transitions, the excitation spectra

also revealed that the  $\text{Tb}^{3+}$  dopants are surrounded by host lattice environment that enable the electrons to be easily excited by less energetic photons. The broad absorption band centers around 265 nm is believed due to host absorption band in which energy transfer could occur from host lattice phosphor onto the dopant species.

We can also explain the resemblances between the afterglow phosphor samples made from bulk ZnO powder and commercially available ZnO nanopowder. We believed that since there is no organic coating that offers protection, the commercially available ZnO nanopowder tend to

clump together and at high temperature (above 1000°C) such that the boundary domain grain size of these nanoparticles break down and

fusion occurred between these nanoparticles, leading to the formation of bulk ZnO particles and therefore the resemblances.

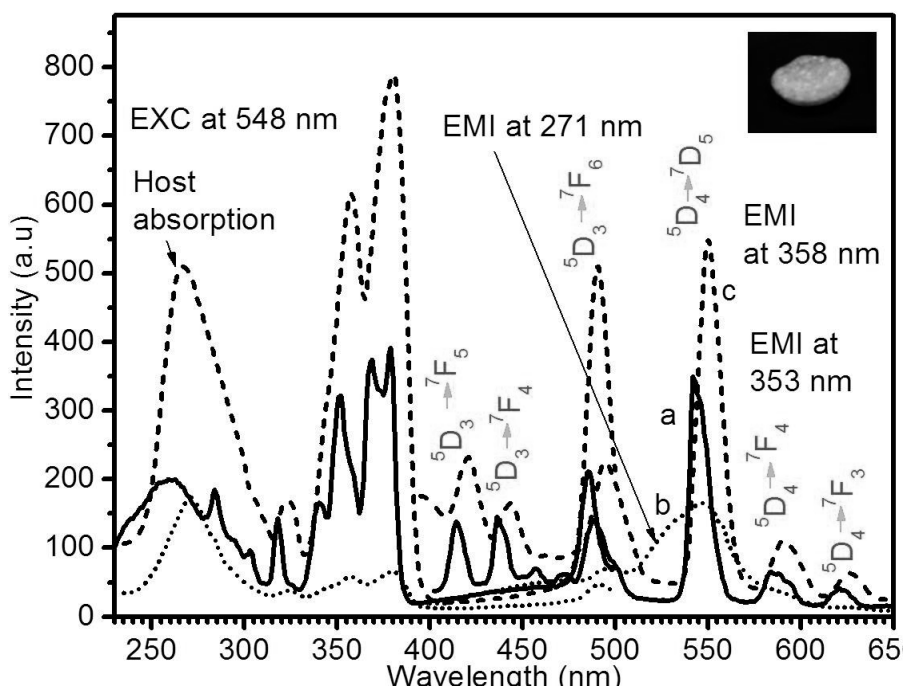


Figure 2. Optical properties of three  $\text{CaZnGe}_2\text{O}_6:\text{Tb}^{3+}$  afterglow phosphors a) 100% gm-weight organic coated luminescence ZnO nanopowder (straight), b) 100% gm-weight bulk ZnO powder (dotted) and c) optimized sample with 70% gm-weight bulk ZnO and 50% gm-weight nano ZnO (dashed). Figure 3 (inset). Optimized  $\text{Tb}^{3+}$  doped sample made of 70% gm-weight bulk ZnO and 50% gm-weight nano ZnO under UVA 350 nm illumination.

From our observations, we are able to conclude that sample made from 100% gm-weight bulk ZnO has these following properties (**Figure 2**). This sample has almost no green  $\text{Tb}^{3+}$  543 nm luminescence upon UVA 350 nm illumination, exhibits UVB afterglow property and tends to be phosphorescence dominant. Meanwhile, the sample made from 100% gm-weight organic coated luminescence ZnO nanopowder has strong green  $\text{Tb}^{3+}$  543 nm luminescence upon UVA 350 nm illumination, weak UVA afterglow property, photoluminescence dominant and excellent luminescence surfaces uniformity. Furthermore, we noticed that the former sample has better UV 254 nm afterglow property compared to the latter sample, this led us to believe that bulk ZnO material contributes to construction of deep well traps in this afterglow phosphor material. We also fabricated samples made with 100% gm-weight organic coated luminescence ZnO nanopowder but with different  $\text{Tb}^{3+}$  dopant concentrations. We found out that with each samples made with increasing

$\text{Tb}^{3+}$  dopant concentration and under UVA 350 nm illumination, the green 543 nm emission tends to become more intense. This is another important observation that led us to believe that more  $\text{Tb}^{3+}$  dopant are being exposed to outside environment due to large surface area of shallow well traps.

Once we have identified the material ingredients responsible for deep well traps and shallow well traps, we decided to fabricate hybrid afterglow phosphors to pursue our investigations. These are afterglow phosphor samples consist of mixture of bulk ZnO and organic coated luminescence ZnO nanopowder. However, before doing so, we need to establish accurately the actual mass of ZnO nanoparticles that are organic-coated. A simple heat treatment experiment is conducted and we established that the actual ZnO nanoparticles' mass is 25.4% of the total gm-weight of the organic coated luminescence ZnO nanopowder. In order to prove that this percentage number is right, we

fabricated a sample made of 70% gm-weight bulk ZnO and 118% gm-weight of organic coated luminescence ZnO nanopowder. This sample turned out as a well-crystallized solid chunk form, permanently fused onto the alumina crucible and has very high hardness, a common property found in metal alloy. This observation verified that the percentage is accurate since the calculation reveal that it fulfilled exactly the total stoichiometric mass for ZnO (0.342 gm from both bulk and nano ZnO), leaving no room for

native internal defects to be formed that could weaken the physical property of the sample. Therefore, at this point, we offer this explanation that if the starting materials consist of mass deficiency in zinc oxide, air chamber enclosure tends to form onto other host lattice layer thus creating structural lattice defect (**Figure 3(b)** and **3(c)**) and this air chamber enclosure's volume is directly proportional to amount of mass deficiency of zinc oxide.

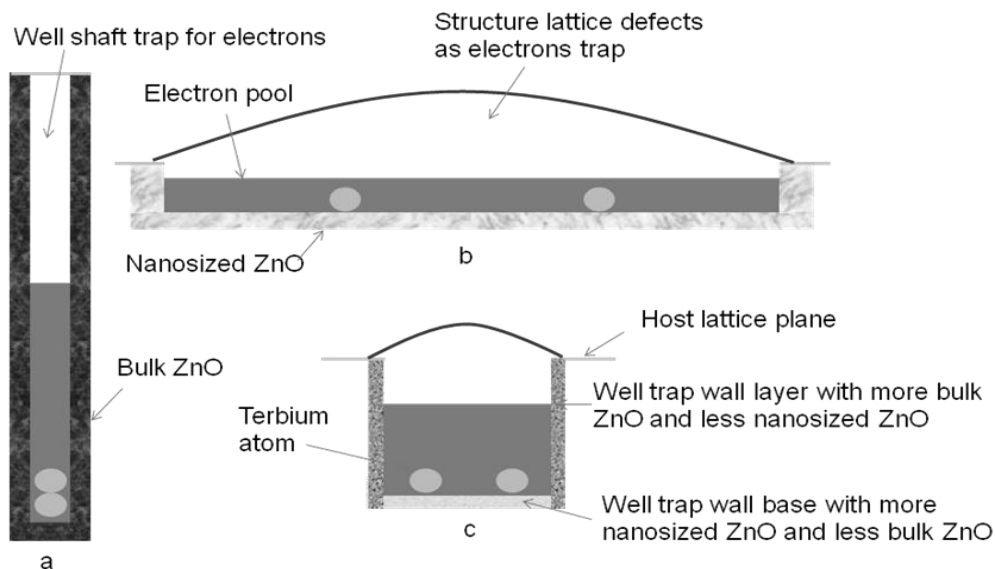


Figure 3. Various well trap structure models based on experimental samples, a) Deep well trap or “Thermos-flask”, 100% gm-weight bulk ZnO b) Shallow well trap or “Frying pan”, 100% gm-weight organic coated luminescence ZnO nanopowder c) Middle-depth well trap or “Hot pot”, the optimized sample with 70% gm-weight bulk ZnO and 50% gm-weight organic coated luminescence ZnO nanopowder.

As the search continues for the hypothetical middle-depth well trap structure phosphor that could give us the best long afterglow duration and with the high temperature furnace pushing at its limit at 1100°C, with no slurry solvent, no ball-milling, and no flux material being employed, the organic coated luminescence ZnO nanopowder prevailed and the final optimized afterglow phosphor sample, was found to be 70% gm-weight bulk ZnO and 50% gm-weight organic coated luminescence ZnO nanopowder. This sample has very good afterglow properties for both UVA 350 nm and UV 254 nm illuminations and it also fluoresces a bright green  $Tb^{3+}$ , 543 nm luminescence upon UVA 350 nm illumination. In order to explain this sample, we calculated the total mass of ZnO required in constructing its well traps to be 0.2828 gm, which is short of the proper

stoichiometric value of 0.342 gm. From this information, we could deduce that the missing ZnO's mass (17.3%) is responsible for creating the inter-layer structure defect which serves as an electron trap for the photo-excited electrons. **Figure 3** shows the various well trap models for this  $CaZnGe_2O_6:Tb^{3+}$  long afterglow phosphor material. First, a straight line is drawn as the host lattice plane if the host lattice phosphor fulfilled the correct mass stoichiometric, this is possible for a sample made of 100% gm-weight bulk ZnO. Two terbium atoms (arbitrarily selected) are added in, at the well trap structure's base to represent for the same  $Tb^{3+}$  dopant concentration used for all three studied samples. Both intrinsic and extrinsic electron contributions from the host lattice phosphor and dopant  $Tb^{3+}$  that are trapped within the well trap structure are labeled as an electron pool. Our first postulate states that bulk

ZnO being responsible for deep well trap structure and phosphorescence dominant agrees with our observation because this deep well trap structure is designed not to receive and radiate light energy easily, a common property found among many long afterglow phosphors, the difficulty of excitation and emission. The second postulate states that the organic coated luminescence ZnO nanopowder being responsible for shallow well trap structure and photoluminescence dominant agrees with our observation because this shallow well trap structure is designed to receive and lose light energy easily or the ease of excitation and emission. If both of these postulates are valid, then it is theoretical possible and experimentally obtainable that a middle-depth well trap structure exists within the host lattice phosphor by adjusting the correct balance of bulk and nanosized ZnO material. This is what the  $\text{CaZnGe}_2\text{O}_6:\text{Tb}^{3+}$  phosphor sample with 70% gm-weight bulk and 50% gm-weight nano ZnO (**Figure 3(c)**, middle-depth well trap structure) constituents represents because this phosphor sample retains the best of both long afterglow and photoluminescence properties and it is easily extractable from the alumina crucible in cohesive solid form. **Figure 3** is proposed in such way so that it has room for improvement, for example,

to determine what exact roles, CaO and  $\text{GeO}_2$  play and also possible sites for point defects and holes trap involving different kind of dopants in future investigations. Hence we conclude that phosphorescence effect is best explained based upon well-trap structure models. It can also be seen from **Figure 3** that the optimized sample's excitation spectra is not well-resolved as compared to sample made of 100% gm-weight nano ZnO, which is another proof due to presence of middle-depth well trap structures within this phosphor material.

**Figure 4** shows the raw XRD diffraction peaks of three undoped  $\text{CaZnGe}_2\text{O}_6$  afterglow phosphor samples. Its structure is monoclinic, with  $a = 1.01737$ ,  $b = 0.90243$ ,  $c = 0.54403$  nm,  $\beta = 105.342^\circ$ , and space group  $C2/c$ . The sharp peaks of all samples indicated that the samples were highly crystallized and with sufficiently larger grain sizes. A more detailed XRD analysis on these new bulk-nano  $\text{CaZnGe}_2\text{O}_6:\text{Tb}^{3+}$  phosphor samples have been discussed and explained in other journal publication [19, see Figure 3 and Table 2], in which the final optimized phosphor sample (70%-50% ZnO) was found to be in  $\text{CaZnGe}_2\text{O}_6$  phase with 91.25 content (wt %).

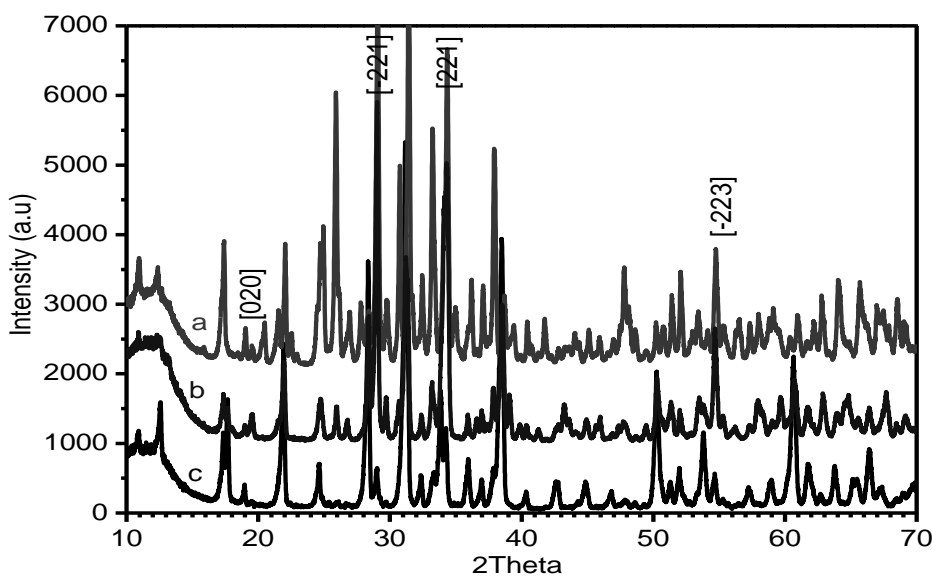


Figure 4. Raw X-ray diffraction patterns of three undoped afterglow phosphor phases a) 100% gm-weight bulk ZnO - $\text{CaZnGe}_2\text{O}_6$  (red) b) optimized sample, 70%-50% gm-weight bulk and nano ZnO -  $\text{CaZn}_{0.83}\text{Ge}_2\text{O}_6$  (blue) c) 100% gm-weight nano ZnO -  $\text{CaZn}_{0.25}\text{Ge}_2\text{O}_6$  (black).

By comparing the physical appearances of all these three studied samples, we noticed that the sample with 100% gm-weight bulk ZnO generally appears in powder form in which we believed is due to lattice compression and strain. Sample with 100% gm-weight nano ZnO may have lattice stretch playing a vital role in determining the internal lattice structural integrity of this sample. As for the optimized sample with 70% gm-weight bulk and 50% gm-weight nano ZnO, this sample's internal lattice structure is much more stable, hence it appears as a cohesive solid form, a possible indication of lattice matching occurrence between the bulk and nano ZnO material, especially on the well trap's wall and base (**Figure 3c**). This explains the smooth bottom surface on the obtained optimized phosphor in its cohesive solid form.

In order to find past publication results among the vast research literature in afterglow phosphor field that could support our afterglow well trap models, we managed to select this one paper for our discussion. In 2002, T. Aitasalo group [20] did an investigative report on the role of lattice defects in influencing the persistent luminescence phenomena on  $\text{Eu}^{2+}$ -doped alkaline earth aluminates however the exact roles that the lattice defect played remained sketchy.

$\text{CaZnGe}_2\text{O}_6$  is a well known self-activated phosphor [21] and by referring to **Figure 5**, a

comparison of optical properties of all the three undoped studied samples, we could see that there is a spectral shift of the green emission 531 nm (bulk ZnO) to 452 nm and 444 nm (luminescence nanosized ZnO). Moreover, the figure clearly shown that the undoped optimized sample (70% gm-weight bulk ZnO and 50% gm-weight nanosized ZnO) has the best capacity to contain more highly energetic hot electrons within its internal lattice structure since its blue 444 nm intensity matched the green 531 nm intensity of the sample made of 100% gm-weight bulk ZnO material. We also believed that the blue 452 nm intensity is lower as compared to the other peaks is due to the presence of more ZnO nanoparticles in constructing the shallow well traps which has the poorest ability in containing highly energetic photo-excited electrons, a possibility in which some of these photo-excited electrons could escape via non-radiative centers. The presence of the small 354 nm excitation peaks as exhibited by samples made with organic coated luminescence ZnO nanopowder corresponded well to the notion that the ZnO nanoparticles are well integrated within the host material since we detected this same excitation peak when we measured the optical properties of the organic coated luminescence ZnO nanopowder. These nanosized ZnO particles could also be responsible for the emergence of the blue (444 nm and 452 nm) emission centers.

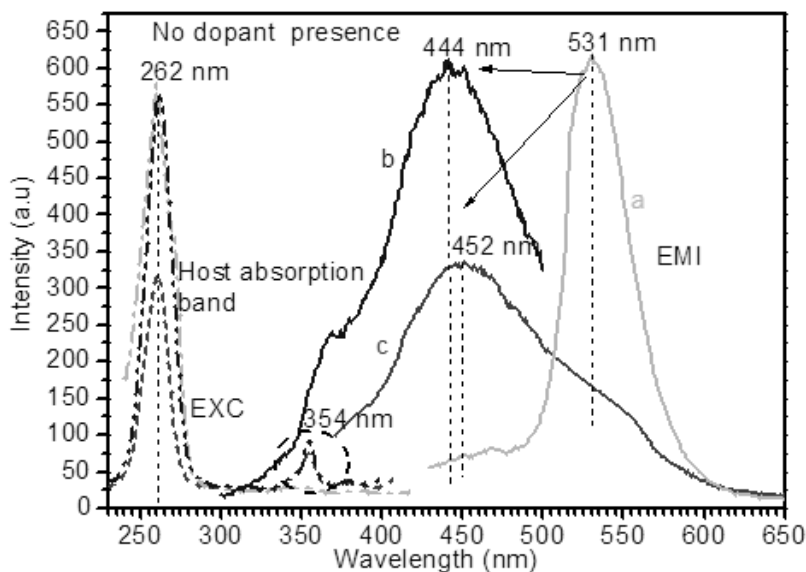


Figure 5. Optical properties comparison between a) undoped sample made of 100% gm-weight bulk ZnO powder (green) b) undoped optimized sample made of 70% -50% gm-weight bulk and nano ZnO (blue) and c) undoped sample made of 100% gm-weight organic coated luminescence ZnO nanopowder (pink).

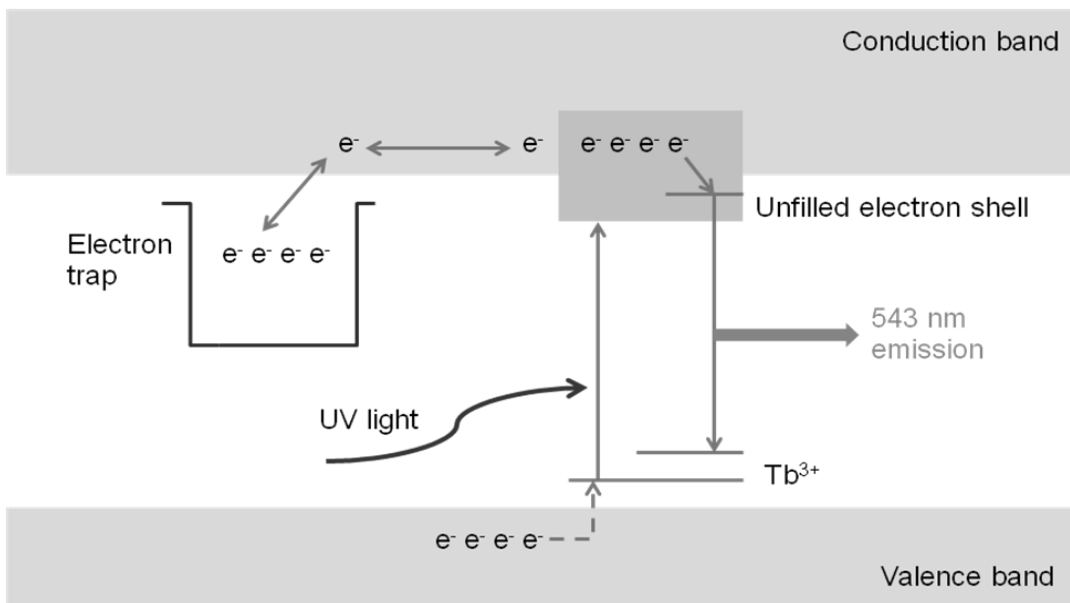


Figure 6. Luminescence mechanism for  $\text{CaZnGe}_2\text{O}_6:\text{Tb}^{3+}$  long afterglow phosphor.

**Figure 6** shows us the luminescence mechanism for  $\text{CaZnGe}_2\text{O}_6:\text{Tb}^{3+}$  long afterglow, the UV light serves to pump out the electrons from the valence band or electron pool of the host material into unfilled electron shell of  $\text{Tb}^{3+}$  dopants which is coincidentally overlaps with the conduction band, these highly energetic photo-excited electrons shall be delocalized when they fall into the electron trap which is located near below the conduction band. After a certain period of time, these trapped electrons or hot electron vapor shall loses their energies, a possibility, in which they come in contact with the structure lattice defects boundary then they shall be released from the trap centers and returned back to certain lower energy states within the  $\text{Tb}^{3+}$  electron shell and fall back to ground state in which recombination with holes in valence band took place, hence emitting the green 543 nm emission as persistent luminescence. The long afterglow decay curve lifetime after illuminating the optimized phosphor sample with mercury lamp (254 nm) for 4 minutes exposure was depicted in **Figure 7**. A proper observation experiment was conducted,

in which we found out that the persistence luminescence can extend over 3 hours period with only 4 minutes exposure time. **Figure 8** shows us the X-ray photoluminescence of this new  $\text{CaZnGe}_2\text{O}_6:\text{Tb}^{3+}$  long afterglow phosphor under 60 kV and 5 mA condition. Sample made of 100% gm-weight bulk ZnO tends to have deep well traps' walls (**Figure 3(a)**) that act as obstacles to the penetrating X-ray beam while sample made of 100% gm-weight nano ZnO has shallow well traps (**Figure 3(b)**) with large surface areas such that the X-ray beam has low probability of hitting and exciting the  $\text{Tb}^{3+}$  dopant, this explains the low X-ray photoluminescence intensity for these both samples. But the optimized sample made of 70% gm-weight bulk ZnO and 50% gm-weight nano ZnO with its middle-depth size well traps (**Figure 3(c)**) has a good balance between the well traps' height and moderate surface area which ensures that the penetrating X-ray beam has high probability of exciting the  $\text{Tb}^{3+}$  dopant, hence this sample exhibits the highest X-ray photoluminescence intensity.

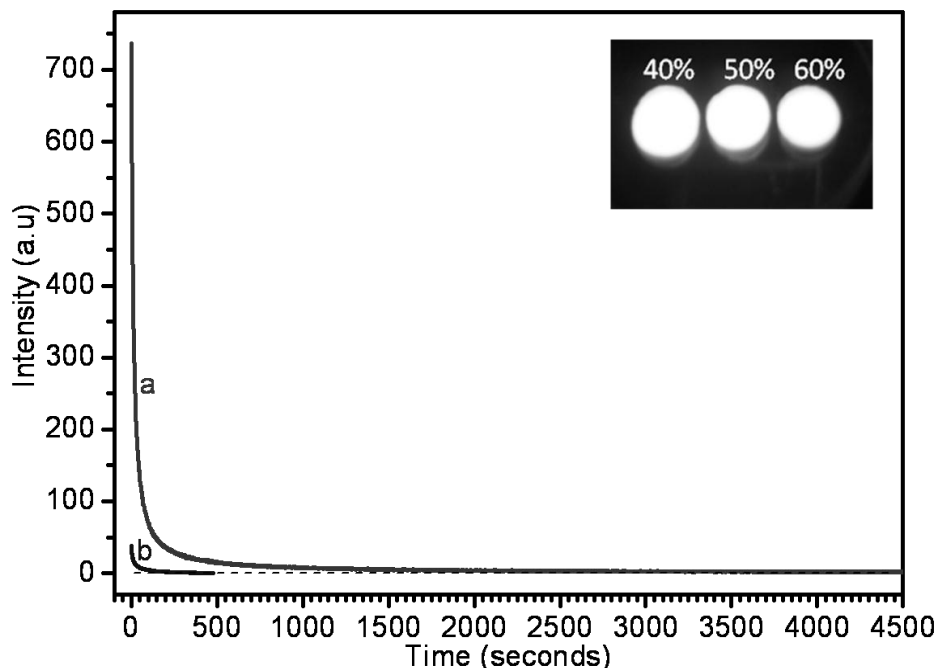


Figure 7. Comparison of afterglow decay curve lifetimes after 4 minutes exposure under mercury lamp source UV 254 nm for a) Optimized  $Tb^{3+}$ -doped sample (70% bulk ZnO - 50% nano ZnO) and b)  $Tb^{3+}$ -doped sample made from 100% gm-weight bulk ZnO.

Figure 9 (inset). Optimized  $Tb^{3+}$  doped samples made from 70% gm-weight bulk ZnO with 40%, 50%, 60% gm-weight nano ZnO under UV 254 nm illumination.

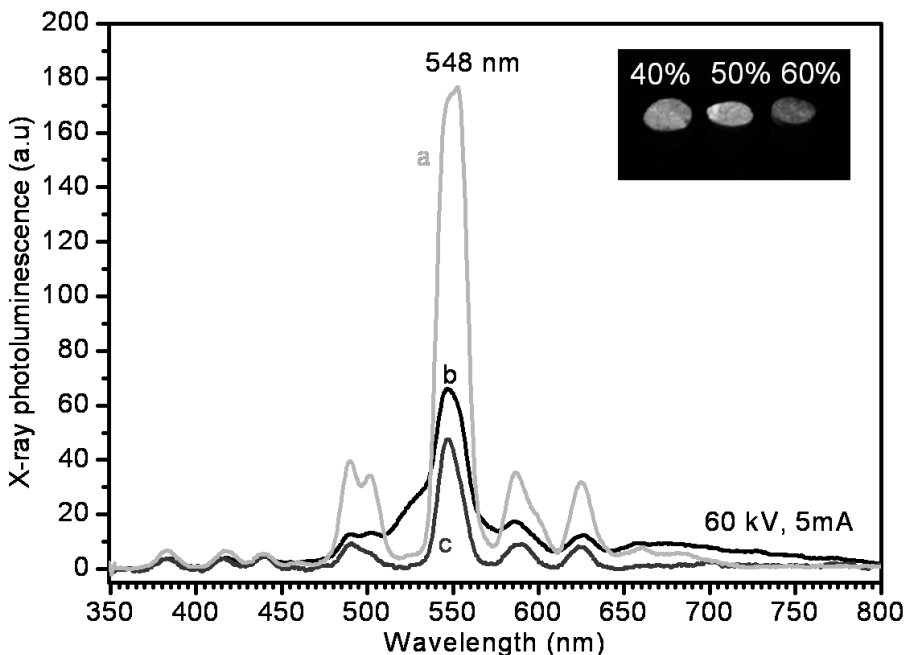


Figure 8. X-ray photoluminescence of three  $CaZnGe_2O_6:Tb^{3+}$  long afterglow phosphor samples: a) optimized sample, 70%-50% gm-weight bulk and nano ZnO (green), b) 100% gm-weight bulk ZnO (black) and c) 100% gm-weight organic coated luminescence ZnO nanopowder (red).

Figure 8 (inset). Optimized  $Tb^{3+}$  doped samples made from 70% gm-weight bulk ZnO with 40%, 50%, 60% gm-weight nano ZnO afterglow in dark after mercury lamp source UV 254 nm is switched off.

## CONCLUSION

In summary, phosphorescence effect of  $\text{CaZnGe}_2\text{O}_6:\text{Tb}^{3+}$  long afterglow phosphor has been optimized by using bulk and nanosized ZnO material. The optimized sample has the constitution of 70% gram-weight bulk ZnO and 50% gram-weight organic coated luminescence ZnO nanopowder or  $\text{CaZn}_{0.83}\text{Ge}_2\text{O}_6:\text{Tb}^{3+}$  phase compound, a middle-depth well trap structure. Based on our experimental findings, we proposed our afterglow well trap structures model to explain persistence luminescence. There are two crucial traps in our models. The first, being the structural well trap that contains the dopant cations and the electron pool. The second, being the air chamber enclosure or structure lattice defects that serves to trap photo-excited electrons. Deep well trap has narrow well shaft trap for electrons that contributes to phosphorescence while shallow well trap has a wide surface area that is enclosed by structure lattice defects boundary which contributes to photoluminescence. By adjusting the right balance of bulk-nano composition of ZnO material, the construction of the middle-depth well trap structure within the host lattice  $\text{CaZnGe}_2\text{O}_6$  phosphor is thus possible. Due to the presence of ZnO nanoparticles within the well traps' bases and walls, the bulk-nano environment they created, contributed in constraining space therefore imposed a strong crystal ligand field within the host lattice material that blue-shifted the host phosphor's green emission. Works are still underway to investigate and to probe deeply the co-dopant issues involving the rare-earth ( $\text{Sm}^{3+}$ ,  $\text{Eu}^{3+}$ ,  $\text{Dy}^{3+}$ ,  $\text{Tm}^{3+}$ ,  $\text{Pr}^{3+}$ ,  $\text{Nd}^{3+}$ ,  $\text{Yb}^{3+}$ ,  $\text{Ho}^{3+}$ ,  $\text{Lu}^{3+}$  etc) and transition metal ( $\text{Mn}^{2+}$ ,  $\text{Cr}^{3+}$ ,  $\text{Sb}^{3+}$ ,  $\text{Bi}^{3+}$ ,  $\text{Mg}^{2+}$ ,  $\text{Na}^+$ ,  $\text{In}^{3+}$ ,  $\text{Ga}^{2+}$ ,  $\text{Ti}^{4+}$ , etc) cations by using our optimized middle-depth well trap model on this  $\text{CaZnGe}_2\text{O}_6$  afterglow phosphor material. Finally, this new  $\text{CaZnGe}_2\text{O}_6:\text{Tb}^{3+}$  long afterglow phosphor has excellent potential to serve as X-ray phosphor by simply tailoring its well traps' depth, active crystal medium for solid-state lasers, highly efficient phosphor for light extraction, tri-dopants approach in obtaining long lasting red afterglow and also with the possibility of advancing triboluminescence field of study.

## ACKNOWLEDGEMENTS

The authors gratefully thank Dr. Marius Hossu for help in X-ray photoluminescence measurements. Special thank to Ken and Gail Spontelli from Mansfield, Texas for proof-reading this research manuscript.

## REFERENCES

1. C. Liu, Y.H.Wang, Y.H. Hu, R. Chen, F. Liao, J. Alloys Compd. 470 (2009) 473-476.
2. L.X.Wang, L. Zhang, Y.D. Huang, D.Z. Jia, J.J. Lu, J. Lumin. 129 (2009) 1032-1035.
3. M. Kowatari, D. Koyama, Y. Satoh, K. Iinuma, S. Uchida, Nucl. Instrum. Methods Phys. Res. A 480 (2002) 431-439.
4. J. Qiu, K. Miura, H. Inouye, Appl. Phys. Lett. 73 (1998) 1763-1765.
5. C. Li, Y. Yu, S.Wang, Q. Su, J. Non-Cryst. Solids 321 (2003) 191-196.
6. Yanqin Li, Yuhua Wang, Xuhui Xu, Yu Gong, Journal of Luminescence 129 (2009) 1230-1234.
7. BingFu Lei, Bin Li, Xiaojun Wang, Wenlian Li, Journal of Luminescence. 118 (2006) 173-178.
8. Boon Kuan Woo, Wei Chen, Alan G. Joly, R. Sammynaiken, Journal of Physical Chemistry C. (2008) 112 14292-14296.
9. Chunbo Liu, Guangbo Che, Zhanlin Xu, Qingwei Wang, Journal of Alloys and Compounds. 474 (2009) 250-253.
10. Pan Weng, Ning Gui-Ling, Wang Jing-Hui, Lin Yuan, Chinese Journal of Chemistry. 25 (2007) 605-608.
11. T. Matsuzawa, Y Aoki, N. Takeuchi, Y. Murayama J. Electrochem. Soc. 143 (1996) 2670.

12. S. W. S. McKeever, in *Thermoluminescence of Solids*, R. W. Cahn, E. A. Davis and I. M. Ward, Editors, Cambridge University Press, Cambridge, England 1985.
13. S. Basun, G. F. Imbusch, D. Jia, and W. M. Yen, *J. Lumin.*, 104, 283 2003.
14. Weiyi Jia, Huabiao Yuan, Lizhu Lu, Huimin Liu, William M. Yen, *Journal of Crystal Growth* 200 (1999) 179-184.
15. D. Jia and W. M. Yen, *J. Lumin.*, 101, 115\_2003.
16. A. A. Setlur, A. M. Srivastava, H. L. Pham, M. E. Hannah, U. Happek, *Journal of Applied Physics* 103 053513 (2008).
17. Dongdong Jia, Weiyi Jia, Yi Jia, *Journal of Applied Physics* 101, 023520 (2007).
18. T. Aitasalo, D. Hreniak, J. Holsa, T. Laamanen, M. Lastusaari, J. Nittykoski, F. Pelle, W. Streck, *Journal of Luminescence*, 122-123 (2007) 110-112.
19. Boon Kuan Woo, Zhiping Luo, Yang Li, Surinder P. Singh, Alan G. Joly, Marius Hossu, Zhongxin Liu, Wei Chen, *Optical Materials*, 33 (2011) 1283-1290, Available online 31<sup>st</sup> March 2011.
20. T. Aitasalo, P. Deren, J. Holsa, H. Jungner, J.-C. Krupa, M. Lastusaari, J. Legendziewicz, J. Niittykoski, and W. Streck, *Journal of Solid State Chemistry* 171 (2003) 114-112.
21. Guangbo Che, Chunbo Liu, Xiuying Li, Zhanlin Xu, Yang Liu, Hang Wang, *Journal of Physics and Chemistry of Solids*, 69 (2008), 2091-2095.